JOURNAL OF PROPULSION AND POWER
Vol. 21, No. 5, September–October 2005

Thermal Decomposition of Hydrogen Peroxide, Part 1: Experimental Results

J. S. Mok*
Hyundai Motor Company and Kia Motors Corporation, Hwaseong-Si 772-1, Republic of Korea
W. J. Helms†
NASA Johnson Space Center, Houston, Texas 77058
and
J. C. Sisco‡ and W. E. Anderson§
Purdue University, West Lafayette, Indiana 47907

Thermal decomposition is an important process in propulsion systems that use hydrogen peroxide (HP). Neither a combined vaporization–decomposition model nor a fundamental understanding of the way liquid HP vaporizes and decomposes in these rocket applications exist. Results are presented from an experimental study of the combined thermal decomposition of HP at rocket-type conditions. A liquid spray of HP is injected into a cross stream of HP decomposition products at chamber pressures ranging from 2.0 to over 5.5 MPa. Two injectors with different orifice diameters are used. Experimental parameters include flow rates of the decomposition products and liquid injectant, HP concentration, chamber geometry, and momentum ratio between the liquid injectant and the decomposition stream. A decomposition efficiency of the liquid HP is determined based on the ratio between measured chamber pressure and chamber pressure calculated by equilibrium chemistry. An analysis of the crossflow injection is used to assess the effects of spray trajectory. Decomposition efficiencies ranging between 10 and 90% were measured. The results show that decomposition efficiency is inversely proportional to the fractional amount of liquid injectant flow rate, linearly proportional to residence time, and that higher concentration HP decomposes at a faster rate.

Introduction

HYDROGEN peroxide (HP) is an attractive propellant due to its low toxicity, storability, high-density impulse, and versatility. The decomposition of HP is an important factor in any HP-based propulsion application. In terms of generating hot gas for propulsion, rapid decomposition of HP is obviously desirable. Its heterogeneous decomposition in the presence of a variety of catalysts such as silver, platinum, ruthenium, and various metal oxides is well known,[1] and this knowledge has led to successful catalyst bed designs. The past decade has seen renewed efforts in developing fuel–catalyst combinations that react spontaneously with HP.[2–4] However, a second important decomposition mechanism, thermal decomposition, remains largely unstudied in its application to propulsion. Thermal decomposition comprises the simultaneous processes of liquid-phase heating and decomposition, vaporization, and vapor phase decomposition.

Thermal decomposition occurs in the aft end of conventional catalyst beds, in thermal decomposition chambers, during bipropellant reaction in combustion chambers, in liquid film cooling layers, and, to some degree, in flow channels in regeneratively cooled combustion chambers. The direct practical application of thermal decomposition is a staged decomposition system, whereby the peroxide flow is split between a heterogeneous catalyst bed and downstream liquid injection.

This paper provides results from an experimental study of the decomposition of high-concentration liquid HP that is injected into a separate stream of decomposition products at elevated chamber pressures. The decomposition product stream was produced from the flow of a mixture of 90% HP and 10% water (by weight) through a catalyst bed. Liquid injectant decomposition efficiencies were derived from measurements of characteristic exhaust velocity efficiency. Experimental parameters included liquid injectant HP concentration, mass and momentum ratios of liquid peroxide to decomposed peroxide, chamber residence time, and liquid injector design.

Decomposition Process

The thermal decomposition of HP can occur either through homogeneous or heterogeneous reactions.[1] Heterogeneous reactions are catalyzed by material surfaces, such as walls, catalyst beds, or reactive particles in the flow. Homogeneous reactions are single-phase processes. Detailed studies of decomposition are complicated by the extraordinary sensitivity of the decomposition process to slight changes in the physical nature of the containment vessel and in the fluid itself. Note that all high-concentration peroxide commercially available for propulsion applications contains significant amounts of other chemicals, including stabilizers, corrosion inhibitors, and residuals from the manufacturing process, as well as somewhere between 2 and 10% by weight of water. The effects of these minor constituents must be considered.

All HP decomposition processes are alike in that the overall production of gaseous products from liquid HP can be written as $2H_2O_2 \Rightarrow 2H_2O + O_2$, which is an exothermic reaction with a heat of decomposition of 2884.5 kJ/kg (1240.1 Btu/lb) of the pure compound. Schumb et al. describe self-sustaining thermal decomposition in Ref. 1 (page 180) as follows:

> If a concentrated aqueous hydrogen peroxide solution is heated to a temperature at which the vapor produced lies within the explosive composition range, it is possible to ignite the vapor and

Presented as Paper 2002-4028 at the AIAA/ASME/SAE/ASEE 38th Joint Propulsion Conference and Exhibit, Indianapolis, IN, 7–10 July 2002; received 7 September 2004; revision received 22 February 2005; accepted for publication 23 February 2005.

*Engineer, Emission Research Team Advanced Technology Center.
†Aerospace Systems Technologist, Mission Operations Directorate, Systems, Division, Guidance and Propulsion Branch, Space Shuttle Guidance and Controls Group.
‡Graduate Research Assistant, School of Aeronautics and Astronautics.
§Assistant Professor, School of Aeronautics and Astronautics.

> produce a continuously-propagating flame . . . the vapor can be ignited by a spark, hot wire, or catalytically-active surface . . . heat transferred down from the flame causes continuous vaporization of the liquid, and the flame will continue to "burn" quite evenly without supply of any external heat.

At atmospheric pressure, the vapors containing 26 mole% or more HP are in the explosive range. This corresponds to liquid weight concentrations of 74% at its boiling point.

Thermal decomposition in the liquid phase has essentially been neglected in propulsion application studies. Because of its very low vapor pressure, HP drops could be heated to relatively high temperatures, for example, the saturation temperature at 22.0 MPa (3200 psia) is 730 K (850°F), before vaporization occurs, thereby increasing liquid-phase decomposition rates.

Unpublished safety and manufacturing data from Food Machinery and Chemical Corporation (FMC), a leading manufacturer of HP, indicate a pre-Arrhenius constant A of 7020 s^{-1} and an activation energy E_a of 79.3 kJ/mole in clean aluminum storage vessels. These data indicate homogeneous liquid-phase decomposition reaction half-times [$\tau_{1/2} = \ell_n(2/k)$, where $k = A\exp(-E_a/RT)$] on the order of seconds for typical boiling points. If infinitely fast heat conduction through the liquid phase is assumed, the liquid-phase temperature rise is only about 10 K for every 1% of decomposition. It is more likely, however, that the liquid-phase decomposition could cause very high local heating rates and possibly explosive gasification. In detailed studies of similar high-energy density propellants, such as hydroxyl ammonium nitrate (HAN) and certain types of organic azides, increased gasification rates and microexplosions have been reported.[5–7] Whereas faster vaporization and small drops can certainly lead to increased performance, high-energy release density and drop shattering have also been widely indicated as likely causes of combustion instabilities in bipropellant rocket engines.

Experimental studies[1,8,9] of vapor-phase decomposition generally indicate that there is a shift from heterogeneous reactions to homogeneous reactions at a temperature of about 700 K (800°F). Because the adiabatic decomposition temperature of 90% HP is about 1010 K (1360°F), and the boiling point of pure HP ranges from about 580 K (580°F) at 3.45 MPa (500 psia) to 720 K (840°F) at 20.7 MPa (3000 psia), homogeneous vapor-phase decomposition reactions should dominate at conditions typical of propulsion combustor/reaction chamber applications.

Whereas previous experimental studies are generally in agreement that the activation energy of the homogeneous reaction is about 0.2 MJ/mole, there was disagreement on the reaction order, as well as on the pressure dependence of the rate constant. A low estimate of the rate constant can be obtained by assuming a first-order reaction, using the atmospheric pre-Arrhenius factor obtained by Hoare et al.[10] ($A = 2.5 \times 10^{15}$ s^{-1}), and approximating the film temperature surrounding the peroxide drop as the average of the decomposition temperature and the drop temperature (boiling point) at a representative chamber pressure of 3.45 MPa (500 psia). These assumptions yield a limiting estimate for the homogeneous rate constant of 180 s^{-1} and a reaction half-life of 3.8 ms, which corresponds roughly to the chamber residence time in our studies.

Experimental Approach

Facility and Test Article Description

Experiments were performed at test stand A at the Purdue Advanced Propellants and Combustion Laboratory. A schematic of the configuration employed in the subject testing is shown in Fig. 1. In Refs. 11 and 12 additional details are provided regarding the facility and test approach.

Data acquisition and valve control is performed using a 400-MHz computer running LabVIEW software. Valve control is done by sending on/off signals to a 32-channel relay board via a digital input/output card in the computer. The data acquisition card allows for a total collection capability of 200,000 samples per second of

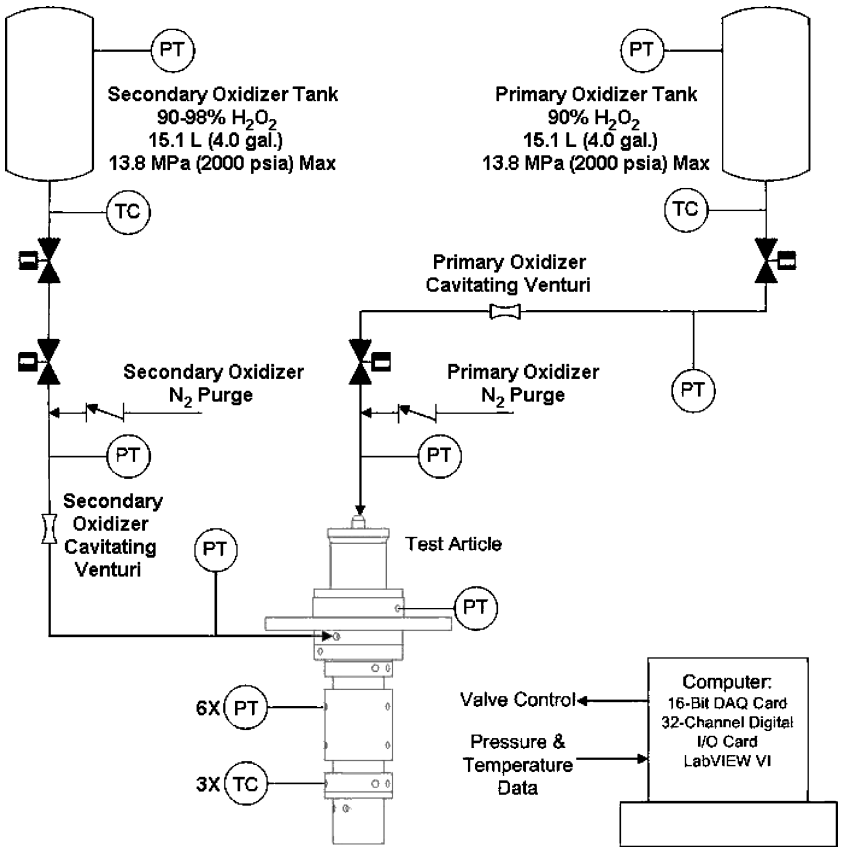

Fig. 1 Experimental schematic; primary oxidizer tank containing 90% HP feeds catalyst bed, and HP at 90–98% HP is fed from secondary oxidizer tank to crossflow injector; pressure transducer (PT) and thermocouple (TC) locations indicated.

32 single or 16 differential analog inputs at a resolution of 16 bits. The pressure transducers were 1000-psia pressure transducers made by Druck. Type-K unshielded thermocouples made by the Omega Corporation were used to measure temperature. The sampling rates were 100 s^{-1}.

HP entered the test article at two locations: a primary flow of 90% concentration by weight entered a silver screen catalyst bed where it was decomposed and then sent into the chamber; a secondary flow of liquid (either 90 or 98% concentration by weight) entered a ring injector through which it was sprayed into the exhaust from the catalyst bed. A General Kinetics catalyst bed (Model P/N GK-GK-PD014-201-001), capable of decomposing up to 0.45 kg/s of 90% HP, was sealed to the injector assembly using knife-edge grooves and a ring of copper sheet. Primary and secondary flows of HP were independently controlled by propellant tank pressure and cavitating venturis. The cavitating venturis were calibrated to measure an effective discharge coefficient. The HP composition was measured by refractometry.

The injector assembly (Fig. 2) was made of two stainless-steel components. The injector body formed the structural portion of the injector and provided inlet ports for the HP supply lines and the outer part of the manifold. Two separate transverse injector rings, designated as injectors A and B, were fabricated for insertion into the injector body. Figure 2 shows one of the stainless-steel rings that was sealed against the injector body using Viton O-rings. Each injector ring used 10 drilled orifices to inject liquid HP radially into the decomposed stream from the catalyst bed. A cross section of the injector ring is shown in Fig. 3.

The modular design was used so that components could be easily changed to allow parametric investigation. The chamber–injector interface was located 12.7 mm (0.5 in.) downstream of the injection plane. Three straight cylindrical sections were made from copper bar stock, one 50.8-mm- (2.0-in.-) long section and two 0.102-m- (4.0-in.-) long sections. Different stacking of the straight cylindrical sections could provide 0.102-, 0.152-, 0.203-, or 0.254-m (4.0-, 6.0-, 8.0-, or 10.0-in.) straight section lengths. Different throat sections allowed changes in contraction ratio (CR) (ratio of chamber area to throat area), which, in turn, allowed changes in gas Mach number and changes in chamber length while maintaining a constant gas residence time. The gas residence time is closely related to the characteristic length L^*, which is the ratio of chamber volume to throat area. Table 1 lists the test configurations.

A 0.102-m chamber section is shown in Fig. 4. An assembly schematic is shown in Fig. 5. Each section was heavily ported for pressure transducers and thermocouples to allow axial profile measurements, although only bulk chamber pressure measurements (PC1 in Fig. 5) were used for the present study. The overall assembly was held together using 10–24 all thread.

Mass flow rates of primary and secondary flows were controlled by a combination of cavitating venturi diameter and run tank ullage pressure. Whereas most tests were performed using 90% HP for the secondary injection, some tests used 98% peroxide to determine the effect of concentration on decomposition. HP was acquired from the FMC. The safe handling and usage of hydrogen peroxide was done in accordance with the aeronautical and astronautical engineering hydrogen peroxide training manual.[13] Properties of HP and its decomposition products are given in Table 2.

Test Procedure

Tests began by acquiring 2 s of zeroing data that were later used to take out biases in the instrumentation data. Because the tests were done in a remote cell, they were viewed during the firings using two

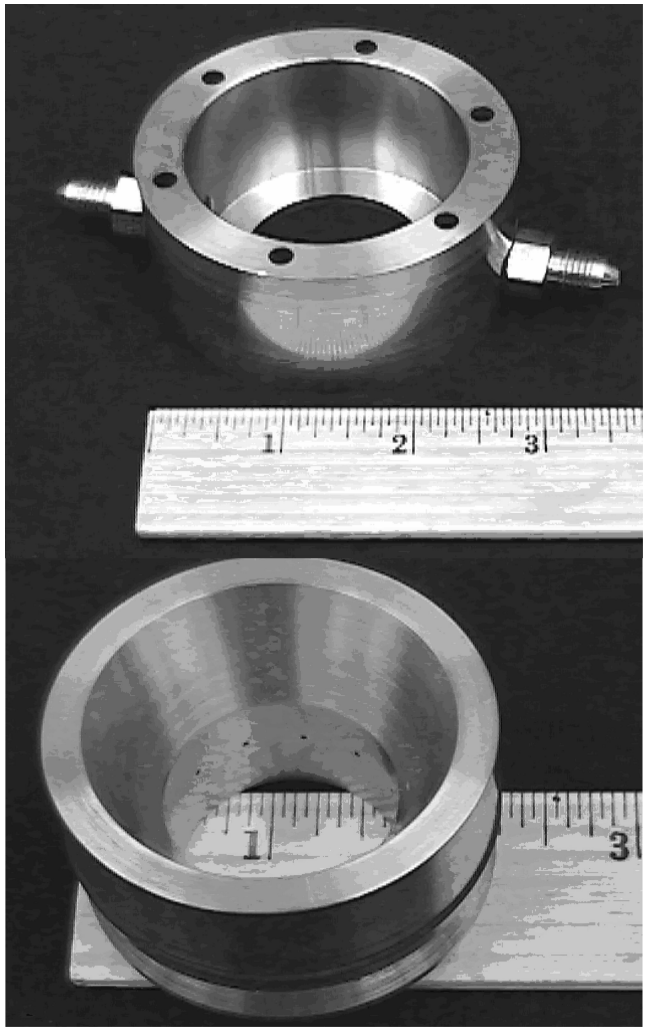

Fig. 2 Injector assembly comprising injector body (top) and transverse jet injector ring (bottom).

Table 1 Chamber configurations used in testing

Injector D_o, mm (in.)	L_c, m (in.)	D_t, mm (in.)	L^*, m (in.)	Contraction ratio $(D_c/D_t)^2$	Nozzle convergence half-angle, deg	No. of tests
A, 0.91 (0.036)	0.102 (4.00)	13.72 (0.540)	0.60 (24.0)	4.9	21.0	4
A, 0.91 (0.036)	0.152 (6.00)	13.72 (0.540)	0.86 (33.9)	4.9	21.0	3
A, 0.91 (0.036)	0.152 (6.00)	10.77 (0.424)	1.38 (54.5)	8.0	24.0	16
A, 0.91 (0.036)	0.254 (10.00)	12.75 (0.502)	1.38 (54.5)	5.7	22.0	1
B, 0.61 (0.024)	0.152 (6.00)	13.72 (0.540)	0.86 (33.9)	4.9	21.0	2
B, 0.61 (0.024)	0.152 (6.00)	10.77 (0.424)	1.38 (54.5)	8.0	24.0	5
B, 0.61 (0.024)	0.203 (8.00)	11.79 (0.464)	1.38 (54.5)	6.7	23.0	2
B, 0.61 (0.024)	0.254 (10.00)	12.75 (0.502)	1.38 (54.5)	5.7	22.0	2

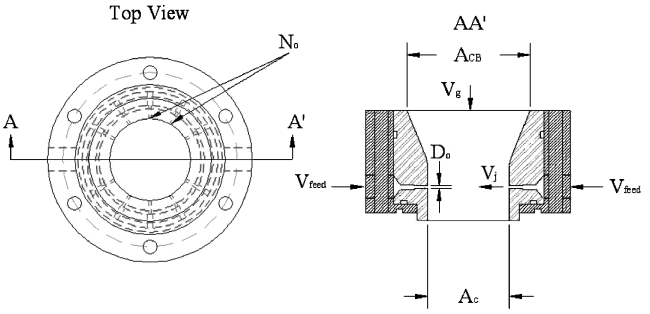

Fig. 3 Cross sections of ring injector, liquid HP injected through 10 radial orifices, two injectors tested, A and B, with orifice diameters D_o of 0.91 and 0.61 mm (0.036 and 0.024 in.), respectively; chamber diameter at the injection plane is 30.5 mm (1.2 in.).

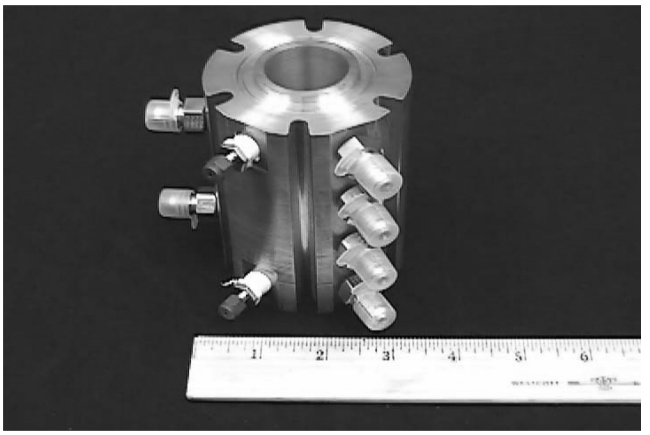

Fig. 4 Straight section of modular chamber.

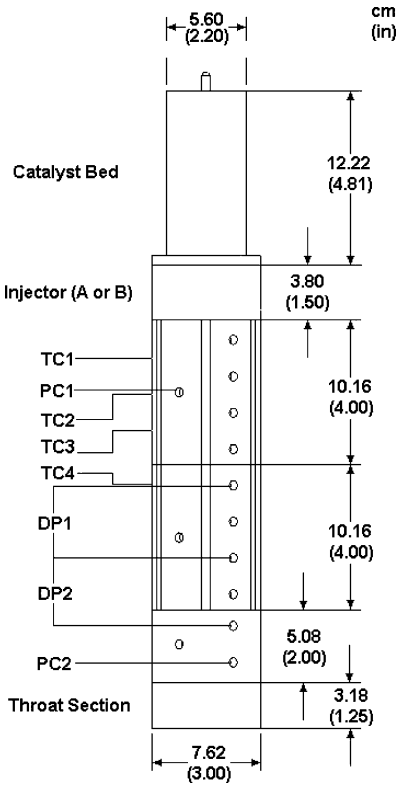

Fig. 5 Assembly schematic of modular chamber, showing only straight sections, dimensions are in centimeters (inches): thermocouple (TC), pressure transducer (PC), and differential pressure measurement (DP) locations noted.

Table 2 Properties of high-concentration HP at 0.1 MPa

Property	90%	98%
Liquid		
Composition by weight	90% HP/10% H_2O	98% HP/2% H_2O
Specific gravity @ 20°C	1.40	1.45
Decomposition products		
Temperature, K (°R)	1022 (1840)	1222 (2200)
Molecular weight	22.1	22.6
Specific heat ratio	1.27	1.25
Characteristic exhaust velocity c^*, m/s (ft/s)	936 (3071)	1018 (3340)

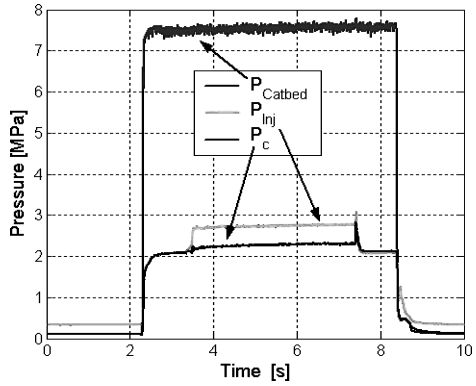

Fig. 6 System pressures for typical test sequence, P_{catbed} is supply pressure to catalyst bed, P_{inj} is pressure in injector manifold, and P_c is chamber pressure.

monitors and video cameras. A nitrogen purge was used to ensure that the lines were free from any propellant, except during the times that the run valves were activated. Check valves were used to shut off the purge during the propellant flow. Before the actual test, a few short pulses of HP were sent through the catalyst bed to warm it up to ensure complete decomposition of the primary flow. The primary test firing was then initiated.

Catalyst bed supply pressure, liquid HP manifold pressure, and chamber pressure measured during a typical test sequence are shown in Fig. 6. During the test, the catalyst bed was run for 6–7 s. The secondary injection of liquid HP began about 2 s after the primary flow, and lasted for about 4 s. A rise in chamber pressure of about 0.1 MPa due to the injection of liquid HP can be seen at about 3 s in Fig. 6. The primary flow through the catalyst bed continued for about 1 s after termination of the secondary injection to prevent any backflow into the catalyst bed. After each test, a shorter firing was performed to expend any remaining propellant in the tanks. Once all propellants were expended, the system was vented and the test cell was opened. The test article, stand, and test video were all inspected.

Results

A total of 35 tests were conducted with eight different test article configurations, including two different injectors (Table 1). Aqueous HP solutions with two different weight concentrations, 90 and 98%, were used as secondary flows. To discriminate the effects between the two different injector configurations, tests and analyses were conducted; the analysis of the crossflow injector is provided in the next section. Test results are presented in terms of the measured decomposition efficiency of the secondary (liquid injectant) flow. Decomposition efficiency is reported in terms of characteristic exhaust velocity c^* efficiency.

The major assumptions made in computing efficiency were that the nozzle flow comprised the decomposed products of the primary and secondary streams only, that the products were in a chemical equilibrium state, and that there was insignificant heat loss to the chamber.

The experimentally measured c^* (in meters per second) was defined as[14]

$$c^*_{\text{exp}} = P_c A_t / \dot{m}_{\text{tot}} \tag{1}$$

where P_c is the chamber pressure, A_t is the throat area, and $\dot{m}_{\text{tot}}$ is the total mass flow rate. The total efficiency η_{tot} is then

$$\eta_{\text{tot}} = c^*_{\text{exp}} \big/ c^*_{\text{theo}} \tag{2}$$

where c^*_{theo} was determined from equilibrium thermochemistry. Thus, the total efficiency is a function of the measured chamber pressure,[14]

$$\eta_{\text{tot}} = P_{c,\text{exp}} / P_{c,\text{theo}} \tag{3}$$

where $P_{c,\text{theo}}$ is computed from the theoretical c^* value, throat area, and measured flow rates. The total efficiency can be written as a sum of the weighted average of the efficiency contributions from the primary and secondary flows,

$$\eta_{\text{tot}} = x_p \eta_p + x_s \eta_s \tag{4}$$

where x_p and x_s are the mass fractions of the primary (catalyst bed) and secondary (liquid injectant) mass flow rate, respectively. The decomposition efficiency of the primary flow η_p was obtained during the test before the liquid HP injection and was assumed to be constant. The average η_p was 98.0% with a standard deviation of 1.7%. Because η_{tot} was obtained during the secondary injection testing, Eq. (4) could be solved for η_s.

For data reduction, test records were first plotted and studied visually. For each test, an interval over which the measured pressures and flow rates were steady (arbitrarily set at a change no greater than 1%) was selected for data reduction. Efficiencies were calculated at each sampling time over this interval and were averaged over the steady interval.

An analysis was performed to estimate the random error in each calculated value and to determine how random error propagated through to each calculated value. Of specific interest was the uncertainty in liquid decomposition efficiency η_s. The uncertainty calculation method presented by Kline[15] was used. This method is based around the relative uncertainty of a measured quantity and is defined as the variation or random error in the value divided by the measured value itself. In this analysis the bias error was assumed to be negligible.

All pressure measurements were assumed to have an error equal to the accuracy of the pressure transducer. The error in the measurement of the throat diameter of each cavitating venturi was set equal to zero; instead this error was lumped into the estimation of the error in the discharge coefficient. This was also done in estimating the error of the liquid injector orifice diameter and discharge coefficient. All other diameter and length measurements were assumed to have an error of ± 0.13 mm, based on machining tolerances. The oxidizer temperature was measured by a thermocouple and the error was estimated at $\pm 2.2^\circ$C. The measurement of the refractive index of HP was accurate to within ± 0.0005, neglecting human error; this puts the error in the measurement of concentration at approximately $\pm 0.1\%$. Based on these estimations, the calculated average uncertainty in the liquid decomposition efficiency was approximately 9.6%. The highest calculated uncertainty was 12.6% whereas the lowest was 9.3%.

Test results are shown in Figs. 7 and 8 for injectors A and B, respectively. Each point corresponds to an individual test. The decomposition efficiency of the liquid HP, η_s, is shown as a function of the fractional of total mass that is injected as liquid HP, x_s. Results for different chamber characteristic lengths L^* and for the two different liquid HP concentrations are shown.

The general trends shown in Fig. 7 for injector A are that decomposition efficiency increases with increasing L^* and decreases with increasing liquid mass fraction. For an identical geometric configuration, the 98% HP results in significantly higher decomposition efficiency. These trends are not as clear with injector B (Fig. 8), however, especially the effect of liquid mass fraction. In a later section, an analysis of the different jet trajectories from injectors A and B will be provided. The analysis will show that the jets from injector B are still intact at the chamber centerline, whereas injector A jets break up into drops before they reach the centerline. A conjecture will be made that the performance of injector B is affected by the coalescence of liquid streams near the chamber centerline, leading to locally high liquid mass fractions and reduced convective transport due to locally lower temperatures and gas stream deceleration, resulting in lower efficiency.

The effects of the liquid HP concentration are shown more specifically in Fig. 9. In each of these tests, the liquid mass fraction was between 0.32 and 0.35, injector A was used, and the chamber L^* was 1.38 m. Note that secondary flows of 98% concentration HP had decomposition efficiencies that were 20–30% higher than 90% HP. The higher concentration HP will have higher rates of vaporization and decomposition due to the higher temperature of the products

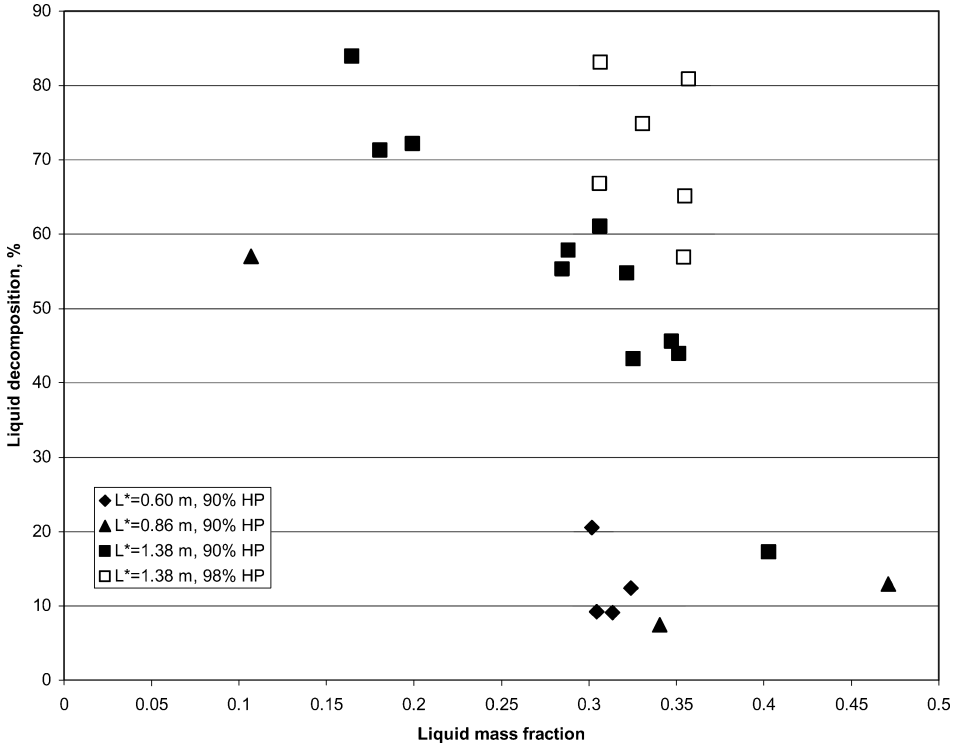

Fig. 7 Liquid decomposition efficiency for injector A for 90 and 98% HP.

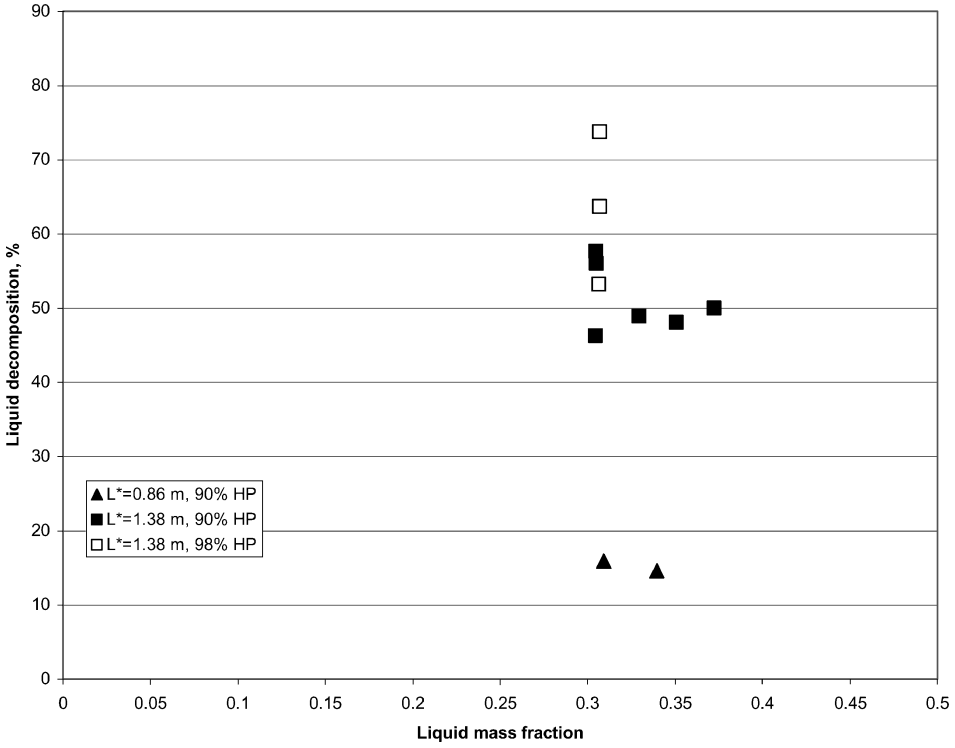

Fig. 8 Liquid decomposition efficiency for injector B for 90 and 98% HP.

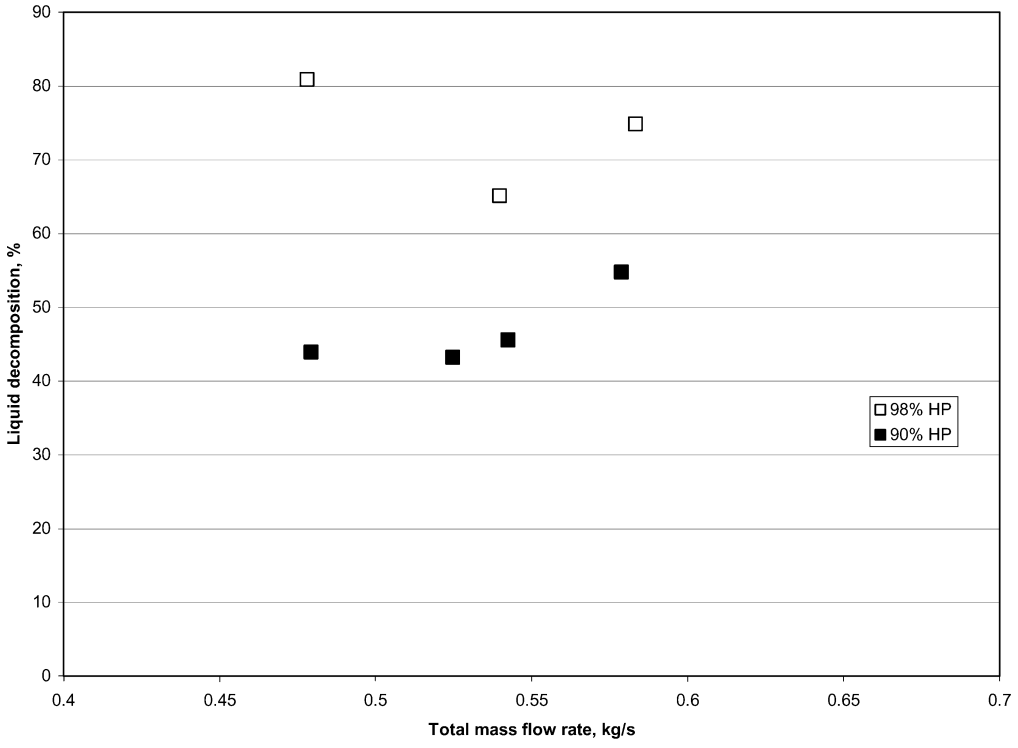

Fig. 9 Effect of secondary flow peroxide concentration on decomposition efficiency for injector A: chamber-to-throat area ratio is 8.0, L^* is 1.38 m, and secondary mass fraction is between 0.32 and 0.35.

of decomposition (equilibrium decomposition temperature of 1222 vs 1022 K) that surround the vaporizing drop, as well as less of a delay during an initial boiloff period when the more volatile H_2O constituent is preferentially vaporizing.

Vaporization and decomposition are dependent on the residence time of the gas in the chamber τ_r. Under the assumption of a perfect gas, τ_r can be written as[14]

$$\tau_r = V_c P_c / \dot{m} R T_c = L^* c^* \Big/ R T_c \tag{5}$$

where V_c is the volume of chamber, T_c is the chamber gas temperature, and R is the gas constant for the HP decomposition products. When Eq. (6) is used to calculate residence time, Figs. 10 and 11 show the strong dependencies of decomposition efficiency on the residence time for both injectors A and B, respectively.

Again, the higher efficiency of injector A is evident. Figure 10 indicates that similar efficiencies are obtained for the 90 and 98% HP at the $L^* = 1.38$ configuration. Note, however, that the higher

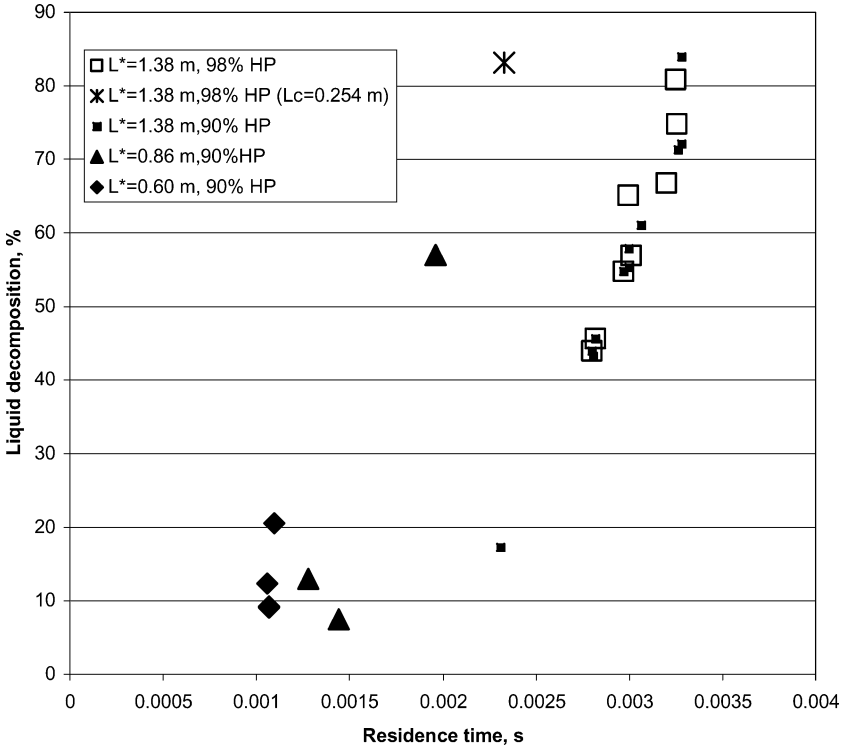

Fig. 10 Effect of residence time on secondary flow decomposition efficiency of injector A.

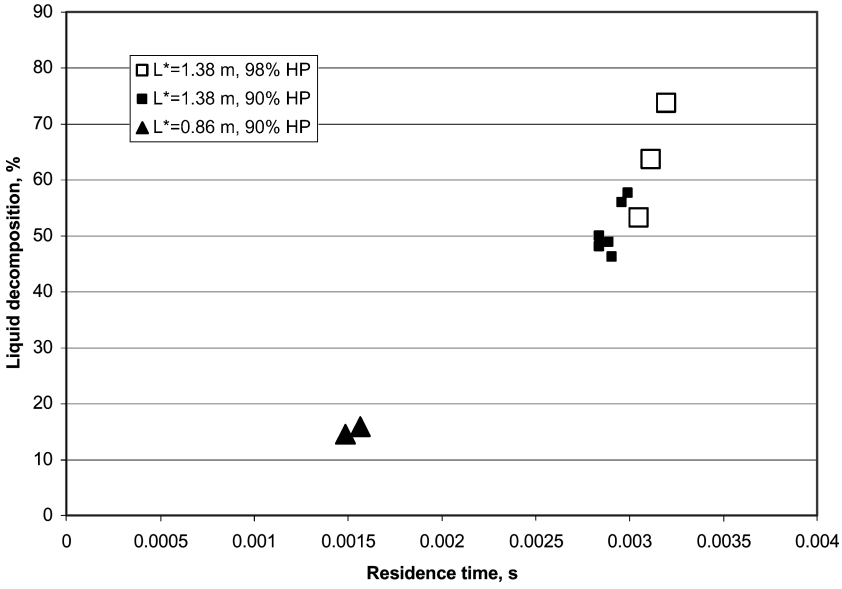

Fig. 11 Effect of residence time on secondary flow decomposition efficiency of injector B.

efficiencies with the 90% HP were achieved with lower mass fraction (Fig. 7).

Other factors affecting decomposition efficiency, mainly through vaporization rate, include initial drop size, the dispersion of the spray, and the convective environment around the liquid drops. Tests were performed to attempt to isolate these effects in terms of the ratio of liquid-to-gas momentum and gas velocity. The momentum ratio Q is known to have a dominant effect on spray formation in a crossflow injector.[16] It is defined as

$$Q = \rho_l V_l^2 \Big/ \rho_g V_g^2 \tag{6}$$

Figure 12 shows decomposition efficiency as a function of Q for all of the tests using 90% HP. An analysis of the effect of Q is given in the next section.

A more specific effect of gas velocity on decomposition efficiency is shown in Fig. 13. In each of these cases, the liquid injection velocities of injector A and B were held constant (within 1 m/s) at 18 and 40 m/s (60 and 133 ft/s), respectively, while maintaining a 0.695/0.305 ratio (within 1%) between the catalyst bed flow and the liquid injectant. The characteristic chamber length L^* was held constant at 1.38 m, and the gas velocity was changed by changing the contraction ratio (CR = 5.7, 6.7, and 8.0). The trends shown in Fig. 13 would indicate that injector A generally provides higher efficiency at the same conditions than does injector B, that efficiency increases with HP concentration (as shown in Fig. 9), and that efficiency increases with increasing gas velocity, except for the two lower efficiency points at gas velocity near 75 m/s. Different plausible explanations for each of these low efficiency points are now presented.

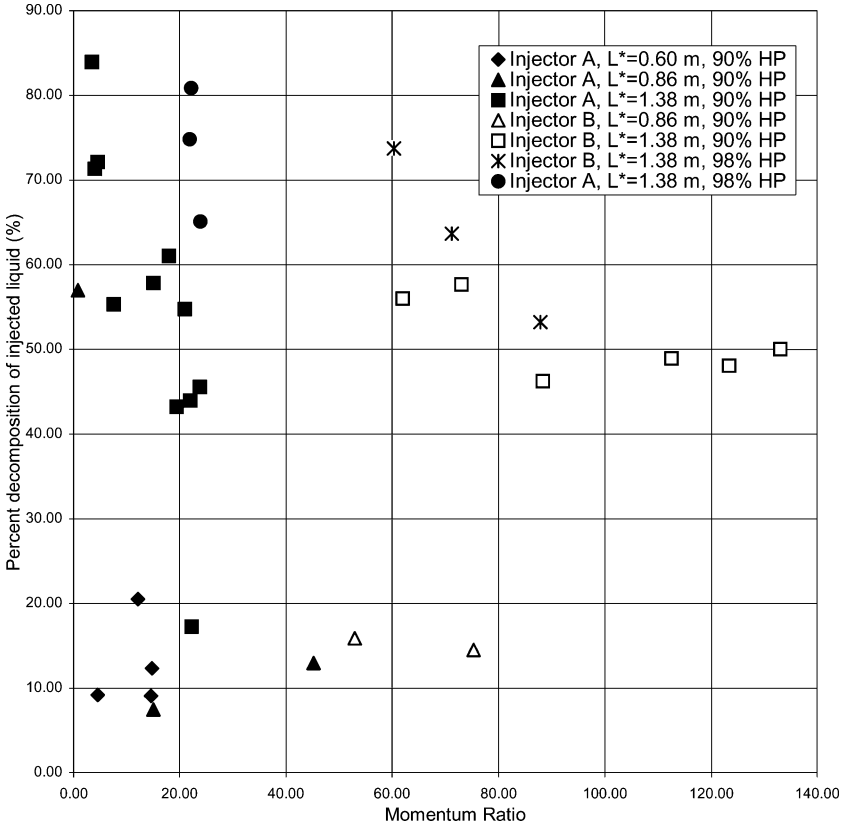

Fig. 12 Effects of momentum ratio Q on decomposition efficiency for 90% HP.

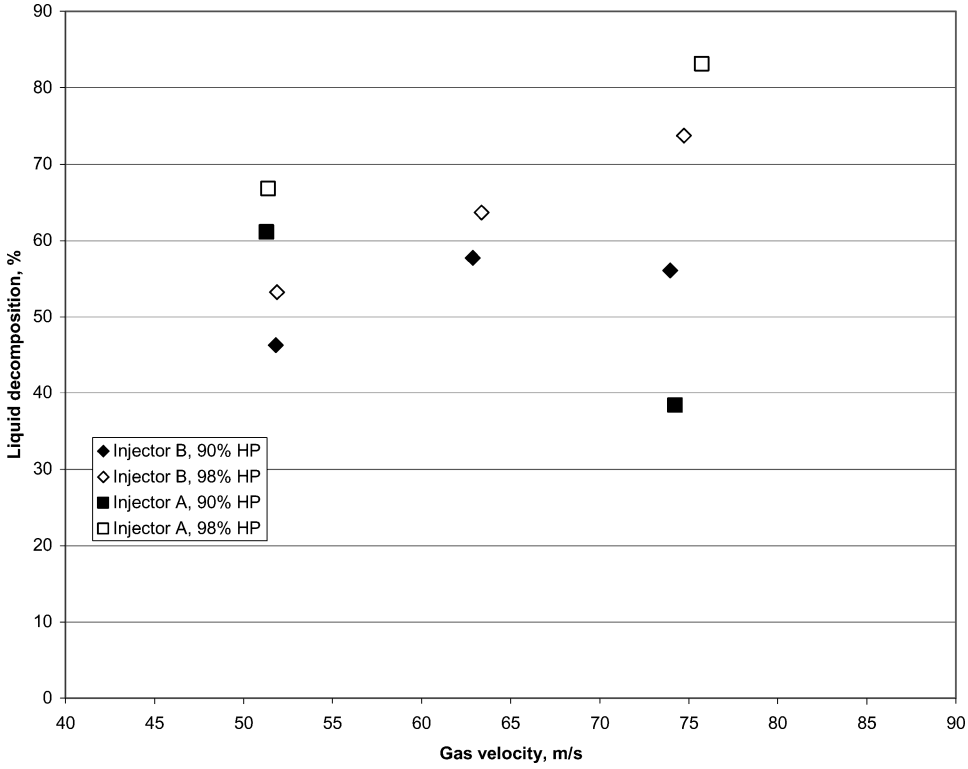

Fig. 13 Effect of gas velocity at injector plane on decomposition of injected liquid HP: total mass flow rate = 0.58 kg/s, mass fraction of secondary flow was between 0.305 and 0.307.

The low efficiency point in Fig. 13 for injector A with high gas velocity was accompanied by strong chamber pressure oscillations. The instability occurred only at this test condition and was demonstrated to be repeatable and intrinsic to the test article (not the test stand). Figures 14 and 15 illustrate the differences between a stable and an unstable test. Both Figs. 14 and 15 show a 0.5-s interval. Note the difference in pressure scales. The stable test shows random pressure fluctuations on the order of a few percent of mean chamber pressure. The unstable test had organized pressure oscillations with a frequency of about 40 s^{-1} and with amplitudes greater than 10% of mean chamber pressure. The cause of the instability is unknown.

To help interpret the other low efficiency point in Fig. 13 (injector B, 90% HP, gas velocity ~75 m/s), as well as why injector A provides higher efficiency than injector B, an analysis of the jet trajectories from each injector was performed to investigate spray dispersion effects. Before the exothermic decomposition reaction, local cooling of the gas flow occurs as the liquid HP drops heat up and vaporize. The greater the local liquid mass fraction, the lower the local gas temperature will be, and vaporization and decomposition rates will be lower. Conversely, a more disperse spray would result in higher decomposition efficiencies.

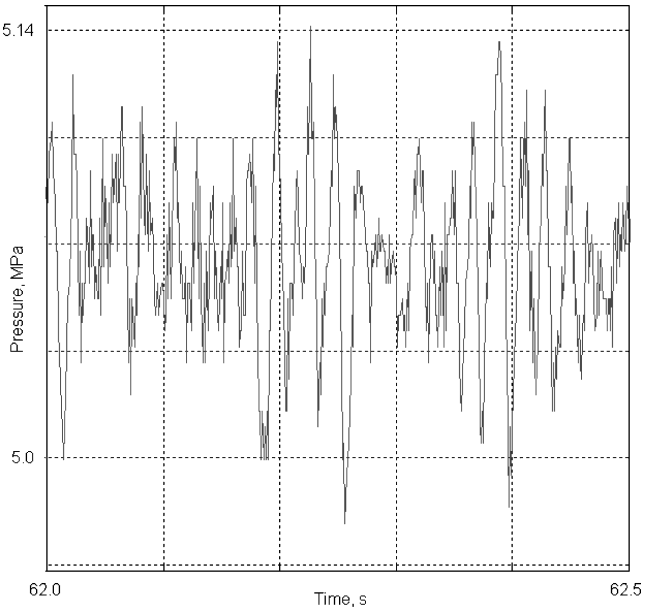

Fig. 14 Typical chamber pressure history showing random pressure fluctuations: mass flow rate 0.58 kg/s, chamber length 0.152 m, and liquid injectant 98% HP.

A correlation developed by Wu et al.[16] was determined to be most applicable to the flow situations encountered during testing. Wu et al. used pulsed shadowgraph imaging to evaluate jet trajectories of water and water/alcohol mixtures in a crossflow. The range of flow parameters experienced during the present study, such as Q, gas Weber number We_{gd}, liquid Weber number We_{ld}, gas Reynolds number Re_{gd}, liquid Reynolds number Re_{ld}, and Ohnesorge number Oh, all fit well within the ranges tested by Wu et al. These parameters are defined as follows:

$$Re_g = \rho_g V_g d_o/\mu_g \tag{7}$$

$$Re_{ld} = \rho_l V_l d_o/\mu_l \tag{8}$$

$$We_{gd} = \rho_g V_g^2 d_o/\sigma_l \tag{9}$$

$$We_{ld} = \rho_l V_l^2 d_o/\sigma_l \tag{10}$$

$$Oh = \mu_l/\sqrt{\rho_l d_o \sigma_l} \tag{11}$$

Here, d_o is the injector orifice diameter, μ_g and μ_l are the dynamic viscosities of the gas and liquid, and σ_l is the surface tension of the liquid. The Ohnesorge number is a measure of the viscous to surface tension forces of the liquid.

Flow parameters for both injectors are summarized in Tables 3 and 4. Tabulated gas velocities are based on monopropellant chamber pressures assuming 100% decomposition efficiency of the primary 90% HP flow, a good assumption due to the consistently high

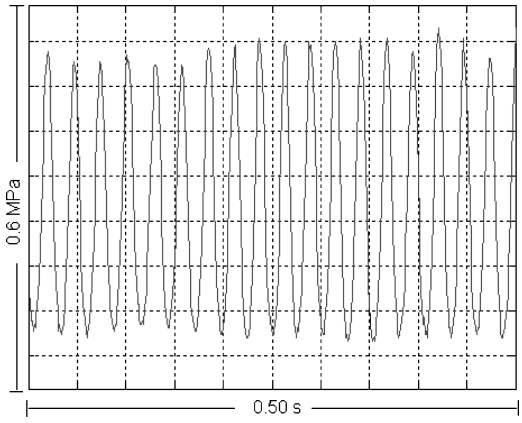

Fig. 15 Unstable condition pressure history: mean chamber pressure was ~3.2 MPa, total mass flow rate 0.58 kg/s, chamber length 0.254 m, and liquid injectant 90% HP.

Table 3 Flow parameters for injector A at conditions in Fig. 13[a]

	CR					
Properties	5.7	6.7	8.0	5.7	6.7	8.0
	90% H_2O_2			*98% H_2O_2*		
Liquid						
V_l, m/s	18.5	18.5	18.5	17.9	17.9	17.9
Re_{ld}	19,000	19,000	19,000	19,200	19,200	19,200
We_{ld}	5,460	5,460	5,460	5,060	5,060	5,060
Oh	3.8e−3	3.8e−3	3.8e−3	3.7e−3	3.7e−3	3.7e−3
Δp_l, psid	34.6	34.6	34.6	33.5	33.5	33.5
Gas[b]						
ρ_g, kg/m^3	7.77	9.10	10.89	7.77	9.10	10.89
V_g, m/s	71.9	61.6	51.5	71.9	61.6	51.5
M_g	0.103	0.088	0.073	0.103	0.088	0.073
Overall						
Re_{gd}	12,500	12,500	12,500	12,500	12,500	12,500
We_{gd}	461	393	329	441	377	315
We_{gr}	491	429	371	469	409	353
Q	11.8	13.9	16.6	11.5	13.4	16.1

[a]Where $d_o = 0.91$ and $N_o = 10$. [b]Decomposed 90% H_2O_2.

Table 4 Flow parameters for injector B at conditions in Fig. 13[a]

	CR					
Properties	5.7	6.7	8.0	5.7	6.7	8.0
	90% H_2O_2			*98% H_2O_2*		
Liquid						
V_l, m/s	41.8	41.8	41.8	40.2	40.2	40.2
Re_{ld}	28,500	28,500	28,500	28,800	28,800	28,800
We_{ld}	18,400	18,400	18,400	17,100	17,100	17,100
Oh	$4.7e{-}3$	$4.7e{-}3$	$4.7e{-}3$	$4.5e{-}3$	$4.5e{-}3$	$4.5e{-}3$
Δp_l, psid	175	175	175	170	170	170
Gas[b]						
ρ_g, kg/m^3	7.77	9.10	10.89	7.77	9.10	10.89
V_g, m/s	71.9	61.6	51.5	71.9	61.6	51.5
M_g	0.103	0.088	0.073	0.103	0.088	0.073
Overall						
Re_{gd}	8,350	8,350	8,350	8,350	8,350	8,350
We_{gd}	307	262	219	294	251	210
We_{gr}	410	383	363	386	359	339
Q	60.0	70.2	84.1	58.1	68.0	81.4

[a]Where $d_o = 0.61$ and $N_o = 10$. [b]Decomposed 90% H_2O_2.

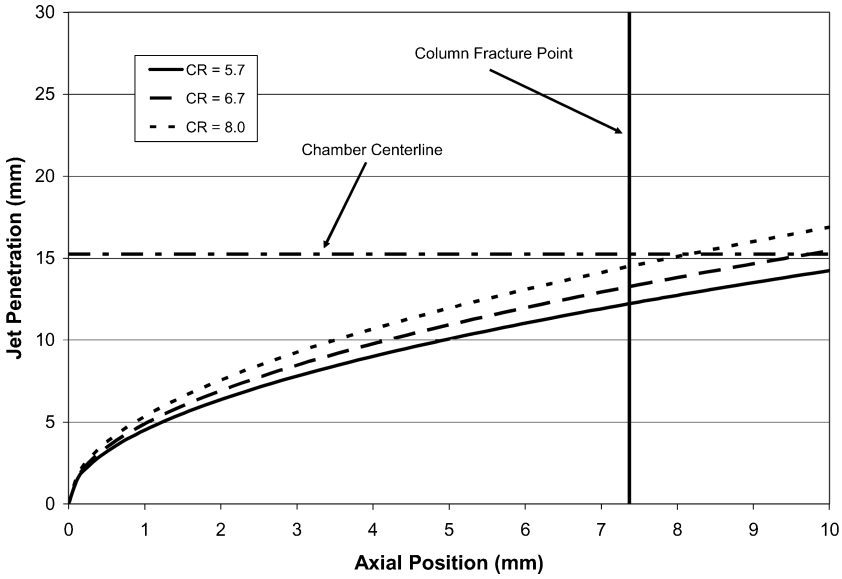

Fig. 16 Liquid jet trajectory as function of CR: baseline test conditions, injector A, secondary injection of 90% HP.

performance of the catalyst bed. The definitions for gas Reynolds number based on chamber diameter Re_g and Weber number based on gas conditions and relative velocity We_{gr} are

$$Re_g = \rho_g V_g D_c / \mu_g \tag{12}$$

$$We_{gr} = \rho_g V_r^2 d_o \big/ \sigma_l \tag{13}$$

where V_r is the relative velocity defined as $(V_g^2 + V_l^2)^{1/2}$. $Re_g = 418{,}000$ at all conditions.

The Wu et al. correlation for jet trajectory is[16]

$$y/d_o = \sqrt{\pi / C_D}\sqrt{Q^x / d_o} \tag{14}$$

They offer the following provisional correlation for drag coefficient C_D based on the range of liquids evaluated in the study:

$$C_D / C_{Dw} = 0.984\,(\mu_l / \mu_{lw})^{0.364} \tag{15}$$

where C_{Dw} and μ_{lw} are the drag coefficient and viscosity for water and are specified as 1.51 and $8.86e{-}05$ kg/m $\cdot$ s. Using Eq. (15) results in drag coefficients of 1.696 and 1.687 for 90 and 98% HP, respectively, at 298 K. The constant term in Eq. (14) was determined to be 1.37 by Wu et al. based on an average C_D of 1.696 for the tested liquids. This agrees very well with the C_D values predicted for the two HP concentrations used in this study, and the following equation was used to predict liquid jet trajectories based on test conditions:

$$y/d_o = 1.37\sqrt{Q^x / d_o} \tag{16}$$

Trajectory profiles based on the test conditions for injector A flowing 90% HP and injector B flowing 98% HP are shown in Figs. 16 and 17, respectively. Note that the higher gas velocity (lower contraction ratio) leads to increased jet deflection. The HP concentration itself has little effect on the trajectory due to a small difference in momentum ratio. The chamber centerline indicated in Figs. 16 and 17 is at the $r = 0$ location at the injection plane (inner diameter $d_c = 30.5$ mm). The column fracture point indicated in Figs. 16 and 17 is the location where the liquid column is predicted to break up into ligaments and droplets. The downstream location x_b where column fracture occurs was calculated according to a correlation also provided by Wu et al.,[16]

$$x_b = 8 d_o \tag{17}$$

No attempts were made to model the drop size distribution that is formed, but many previous studies have indicated a correlation for the Sauter mean diameter (SMD) of the drop size distribution

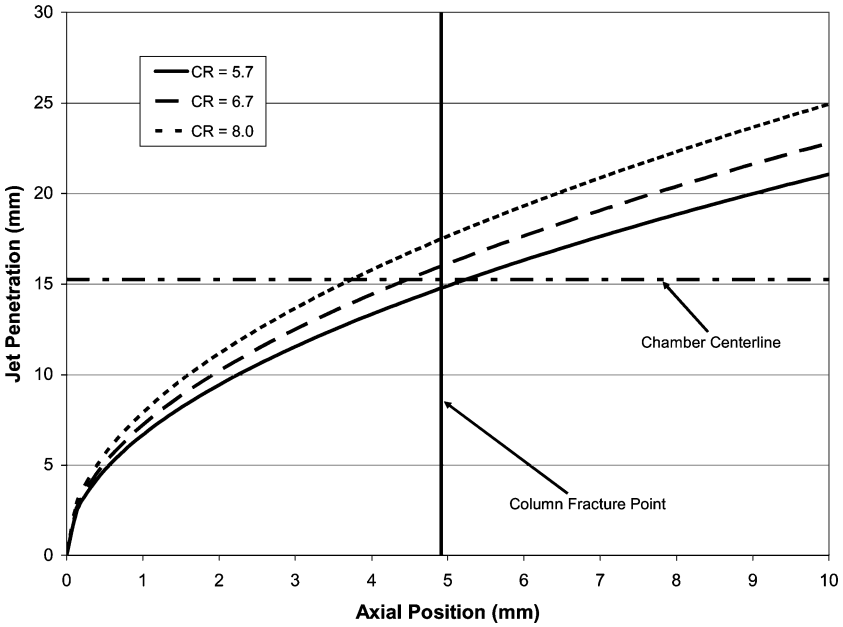

Fig. 17 Liquid jet trajectory as function of CR: baseline test conditions, injector B, secondary injection of 98% HP.

formed by liquid jets in a crossflow that has the following form[17]:

$$\text{SMD} \propto C\sigma^m \Big/ \rho_g^n V_g^p \tag{18}$$

Here, C, m, n, and p are all constants. This equation shows that drop size is proportional to surface tension and inversely proportional to gas density and velocity. The denominator term is similar in form to gas momentum. According to Hautman and Rosfjord,[17] the constant exponent p is larger than n, making the gas velocity the more dominant factor in determining drop size. The correlation given in Eq. (18), along with the fact that the orifice diameter of injector B is smaller than that of injector A, would indicate that the drops formed by injector B should be smaller than those formed by injector A.

Figures 16 and 17 show that the liquid column breaks up before crossing the chamber centerline for injector A, whereas injector B jets cross the centerline, except for the low-contraction ratio case that is calculated to disintegrate near the centerline. Also note that the jets from injector B are predicted to break up earlier than those from injector A. Considering this along with the argument that the drops formed by injector B should be smaller than those formed by injector A would lead to the expectation that injector B should give a higher efficiency.

The calculated trajectories in Figs. 16 and 17 can, thus, be used to interpret the efficiency results shown in Fig. 13 and why injector A gives higher efficiency. The stable, low efficiency point (injector B, HP concentration = 90%, gas velocity ~75 m/s) corresponds to the case in Fig. 17 where disintegration occurs near the centerline. The locally dense liquid fractions near the centerline lead to lower local temperatures due to evaporative cooling effects and slower rates of vaporization. On the other hand, the jets can cross the centerline for the higher Q cases (lower CR cases) with injector B, can disintegrate and disperse, and vaporization can proceed unimpeded by local low gas temperatures. This explanation is also consistent with the fact that the 98% HP presents higher decomposition efficiency than does 90% HP.

Summary

To investigate the thermal decomposition of HP, streams of liquid HP were injected into a gaseous cross stream of decomposed HP products from a catalyst bed. The decomposition efficiency of the liquid HP was measured at moderate chamber pressures while varying the design and operating parameters of liquid mass fraction, liquid-to-gas momentum ratio, gas velocity, chamber residence time, and liquid HP concentration. Efficiency was defined as the ratio of measured chamber pressure to theoretical pressure based on complete decomposition to equilibrium conditions.

There was an inversely proportional relationship between the liquid mass flow rate and the decomposition efficiency of the injected liquid. The increased concentration of HP provided an increase in the decomposition efficiency. Liquid HP decomposition efficiency was proportional to the residence time at efficiencies greater than 40%. At the same liquid flow rate, injector A, with larger injection orifice diameters, lower liquid injection velocity, and lower momentum ratio, gave better decomposition efficiency than injector B with larger smaller orifice diameters.

Effects of gas velocity, which largely determine jet trajectory, drop size, and convective transport rates, were investigated at constant chamber residence time by varying contraction ratio. Trajectory analyses showed that penetration of the liquid jet into the decomposition products from the catalyst bed increased with increasing contraction ratio. Results also showed that jets from injector A did not cross the chamber centerline before breakup, whereas intact jets from injector B penetrated past the centerline. Evidence was provided that higher gas velocity provides increased secondary decomposition rates, allowing for the exceptions of an unexplained instability at a single condition that led to lower efficiency, and significant liquid-phase coalescence near the centerline at another single condition that led to decreased vaporization and decomposition rates.

Most of these effects can be attributed to the amount of heat from the primary flow that is available to vaporize and thermally decompose the secondary flow. Poor liquid-phase dispersion led to locally lower temperatures due to evaporative cooling and lower convective transport rates due to momentum exchange between the drops and the gas. The lower local temperatures also slow the kinetic rate of decomposition. The higher efficiencies measured with the 98% HP can similarly be attributed to a higher vapor film temperature around the drop than those for the 90% drop. It was noted that chemical kinetic times of the vapor-phase homogeneous reaction are on the order of the chamber residence time. More experiments are needed to address specifically the relative effects of vaporization and chemical kinetics as limiting factors.

Acknowledgments

This work was funded by NASA through Grant NAG8-1856, with Amy Reeb as Technical Monitor. The authors wish to thank Amy Reeb of NASA, Scott Meyer of Purdue University for help in the

test setup, Benjamin Austin of INSpace LLC for technical advice, and Madeline Chadwell and Jerry Hahn of the Aerospace Sciences Laboratory for their expert machining of the test articles.

References

[1]Schumb, W., Satterfield, C. N., and Wentworth, R. L., *Hydrogen Peroxide*, Reinhold, New York, 1955, p. 180.

[2]Austin, B. L., and Heister, S. D., "Characterization of Pintle Engine Performance for Nontoxic Hypergolic Bipropellants," AIAA Paper 2002-4029, July 2002.

[3]Long, M. R., Anderson, W. E., and Humble, R. W., "Bi-Centrifugal Injector Development for Hydrogen Peroxide and Non-Toxic Miscible Fuels," AIAA Paper 2002-4026, July 2002.

[4]Hurlbert, E., Applewhite, J., Nguyen, T., Reed, B., Baojiong, W., and Yue, W., "Nontoxic Orbital Manuevering and Reaction Control Systems for Reusable Spacecraft," *Journal of Propulsion and Power*, Vol. 14, No. 5, 1998, pp. 676–687.

[5]Call, C., Zhu, D. L., Law, C. K., and Deevi, S. C., "Combustion and Microexplosion of Han-Based Liquid Gun Propellants at Elevated Pressures," *Journal of Propulsion and Power*, Vol. 13, No. 3, 1997, pp. 448–450.

[6]Li, T. X., Zhu, D. L., and Law, C. K., "Droplet Combustion, Microexplosion, Sooting Characteristics of Several Energetic Liquid Propellants," *Journal of Propulsion and Power*, Vol. 14, No. 1, 1998, pp. 45–50.

[7]Lee, A., Jiang, Y. J., Zhu, D. L., and Law, C. K., "Burning-Rate Enhancement of Organic Diazide Propellants: Dihalide Addition and Pressure Elevation," *AIAA Journal*, Vol. 30, No. 5, 1992, pp. 1298–1303.

[8]Giguere, P. A., and Liu, I. D., "Kinetics of the Thermal Decomposition of Hydrogen Peroxide Vapor," *Canadian Journal of Chemistry*, Vol. 35, No. 4, 1957, pp. 283–293.

[9]Conway, D. C., "Mechanism of the Homogeneous Decomposition of Hydrogen Peroxide," *Journal of Physical Chemistry*, Vol. 61, No. 11, 1957, pp. 1579, 1580.

[10]Hoare, D. E., Protheroe, J. B., and Walsh, A. D., "The Thermal Decomposition of Hydrogen Peroxide Vapour," *Transactions of the Faraday Society*, Vol. 55, 1959, pp. 548–557.

[11]Anderson, W., and Meyer, S. E., "Propulsion Test Facilities at Purdue University," AIAA Paper 2002-4280, 2002.

[12]Mok, J.-S., "Investigation of Simultaneous Vaporization and Decomposition of Hydrogen Peroxide Using Multiple Jets in Crossflow," M.S. Thesis, School of Aeronautics and Astronautics, Purdue Univ., West Lafayette, IN, Dec. 2003.

[13]"Hydrogen Peroxide Training Manual," School of Aeronautics and Astronautics, Purdue Univ., West Lafayette, IN, 2001.

[14]Sutton, G. P., and Biblarz, O., *Rocket Propulsion Elements*, Wiley, New York, 2001, p. 284.

[15]Kline, S. J., "The Purposes of Uncertainty Analysis," *Journal of Fluid Mechanics*, Vol. 107, June 1985, pp. 153–160.

[16]Wu, P. K., Kirkendall, K. A., Fuller, R. P., and Nejad, A. S., "Breakup Processes of Liquid Jets in Subsonic Crossflows," *Journal of Propulsion and Power*, Vol. 13, No. 1, 1997, pp. 64–73.

[17]Hautman, D. J., and Rosfjord, T. J., "Transverse Liquid Injection Studies," AIAA Paper 90-1965, July 1990.